# ELECTROSTATICALLY ACTUATED MICROVALVES FABRICATED WITH SOFT-LITHOGRAPHIC TECHNIQUES FOR INTEGRATED MICROFLUIDICS

BY

JOSHUA TICE

THESIS

Submitted in partial fulfillment of the requirements
for the degree of Master of Science in Chemical Engineering
in the Graduate College of the
University of Illinois at Urbana-Champaign, 2009

Urbana, Illinois

Adviser:

Associate Professor Paul J. A. Kenis

# Abstract

Complex chemical and biological microsystems have the potential to significantly impact point-of-care diagnostics, portable detection systems, and automated, high-throughput chemical processing. The implementation of these systems, however, requires the development of a microvalve that can effectively control connectivity between microfluidic components. Ideally, the valve should be fabricated with simple techniques at low temperature and ambient pressure to facilitate wide dissemination of the technology and also assure effective manufacturability. In addition, the valve should be easily integrated with controls in a portable format.

In this work, I report the development of an electrostatic microvalve that is fabricated with simple, soft-lithographic techniques. An analytical model was developed to guide the fabrication process of the microvalves and also optimize the electrical potentials needed to actuate the microvalves. Several methods were investigated for conferring conductivity to elastomeric membranes, including the patterning of nanoparticle/elastomer composites, the airbrushing of conducting nanoparticle suspensions, and the microtransfer printing of nanoparticle films formed by vacuum filtration. The latter was used to integrate the conducting membranes into a fabrication process for microvalves, which included the incorporation of membrane support structures. The fabrication process was optimized by exploring the design space identified by the model, and the optimization yielded microvalves that actuated with electrical potentials as low as 5 V. The potentials required to operate the valve are low enough that the valve can be directly controlled by electrical integrated circuit chips. Finally, I report the pressures that the microvalves can effectively isolate and the actuation of the microvalves in different liquid media, including fluorinated oils and water.

# Acknowledgements

This work would not be possible without the help and support of many individuals, to whom I am forever grateful. I would first like to thank my adviser and friend, Professor Paul Kenis, for his guidance and for accommodating me before I even joined the graduate program at Illinois. I appreciate the way that he fosters an independent research spirit in all his students, and I look forward to learning much more from him in the future. I would also like to thank Professor Christopher Apblett from Sandia National Laboratories for his mentorship and for the insight that he brought to the project. Several other coworkers and collaborators participated directly in the work, and I thank them for their efforts. Among them are Dr. Amit Desai and Tom Bassett from the University of Illinois, Dr. Gregory Ten Eyck and Dr. Richard Givler from Sandia National Laboratories, and Andrew Collord and Christopher Hamlin from the University of New Mexico. Financial support was provided by the United States Department of Energy and National Science Foundation. I would like to thank several of my classmates and coworkers who provided invaluable input during the course of this project, including Sarah Perry, Benjamin Schudel, Dr. Matthew Cole, Dr. Michael Toepke, and Dr. Tobias Wheeler. Thanks to all the members of the Kenis lab, past and present, for the advice, light-hearted discussions, and adventures in and out of lab. I would like to thank my roommates who provided a community of support for me at home, especially Daniel Kim and Moochul Shin, and I thank my family for their never-ending love and encouragement.

*To my Father*

# Table of Contents

# Chapter 1: Introduction

## 1.1 Integrated Microchemical Systems

In recent years, chemistry in miniaturized systems has been a topic of intense research because of several well-known advantages on the microscale, including enhanced heat and mass transfer (due to steep temperature and concentration gradients and small length scales), increased surface to volume ratio, and the existence of interesting phenomena unique to the microscale (e.g. electro-osmotic flow, which requires surface forces to dominate the normally prevalent inertial forces at the macroscale). A number of microfluidic components have reached a high level of maturity, including mixers [1], separation units [2-4], pumps [5], reactors [6-9], heat exchangers [10], and sensors [7, 11, 12]. However, the full potential of microfluidics lies in the ability to integrate these components into complete systems capable of performing complex chemical operations – essentially creating a "lab-on-a-chip". These integrated microchemical systems will demonstrate drastic improvements over their macroscale equivalents in terms of portability, automation, and parallel processing.

Already, a number of impressive examples of integrated microchemical systems have been reported in literature, including chips designed to isolate and sequence DNA [13], screen for gene expression [14], perform multistep synthesis of a radioimaging probe [15], and screen for protein crystallization conditions [16-18]. All of these systems rely on means of directing the flow of chemical reagents from one microfluidic component to another. While many of these applications require merely a continuous flow where solutions flow serially from one micro- unit operation to the next, clearly

there are many that require more complex connectivity. The one microfluidic component that has made these more complex systems possible is the microvalve.

### 1.2 Microvalves for Integrated Microchemical Systems

There are several criteria that should ideally be met in a microvalve designed for integration into a microchemical system. Firstly, the valve should be simple to fabricate. For this simple fabrication to be realized, the valve should be monolithic with the rest of the device. The greater the number of components that require different materials, the higher the number of serial steps required to fabricate the system. On the other hand, if the valve is composed of the same materials as the rest of device, the valve could be fabricated in-parallel with the other components. In order for the valve to be easily manufactured, the fabrication should be performed at low temperatures, ambient pressures, and with non-specialized equipment (i.e. if possible, without the use of a clean room, high vacuum deposition tools, or high temperature annealing ovens). Secondly, the valve should have a small footprint, allowing a high density of valves. Thirdly, for most applications the valve should actuate rapidly. For a number of applications, rapid actuation may not be necessary or even desirable, but generally the most versatile valves actuate quickly. Lastly, the valve needs to be amenable to effective controls. The controls must also be small and portable along with the rest of the device, and should interface conveniently with the valves. For portable applications, the controls should consume little power to accommodate a portable power supply.

There are numerous examples of microvalves that have been developed for microfluidic applications. Among them are microvalves that are actuated with magnetic

forces, thermal expansion, volume-changing hydrogels, and electrostatics, which have all been thoroughly reviewed by Oh and Ahn [19]. Unfortunately, most of the microvalve examples do not meet all the criteria for valve integration mentioned previously. Most commonly, the valves require intensive fabrication processes, or the valves are not compatible with a wide range of chemical environments (e.g. volume changing hydrogels which are sensitive to pH).

One of the most widely implemented microvalves in integrated microchemical systems is a pneumatic microvalve fabricated entirely from polydimethylsiloxane (PDMS) using soft-lithographic techniques – specifically replica molding (Figure 1.1a) [20]. The fabrication is straightforward and meets most of the criteria for valve integration mentioned previously. Firstly, two molds are made from silicon and photoresist using standard photolithographic techniques. These molds may then be used numerous times thereafter. One of the molds is fabricated with a positive resist, which is then heated and allowed to reflow, forming rounded channels. The second mold is fabricated with a negative resist. A thin layer of PDMS (deficient in cross-linker) is spin-coated over the mold with rounded channels, while a thick layer of PDMS (excess cross-linker) is poured over the mold with rectangular channels. After curing, the thick layer is aligned over the thin layer, and the point of overlap between the upper channel and lower channel defines a valve with a thin membrane separating the two channels (Figure 1.1b). The layers seal together due to the mismatch in the amounts of cross-linker between the two PDMS layers. When a pressure is applied to the channel on the top, the membrane presses down into the channel below, constricting the flow (Figure 1.1c). While there are few examples in the literature of valve fabrication procedures that are as easy, the

pneumatic valves do suffer from one significant drawback, which is the bulkiness of the controls. The valves require a pressurized gas source and an external array of solenoid valves. Also, the interface between the external controls and microfluidic chip is complicated.

Several attempts have been made to simplify the controls of the pneumatic valves by switching to electrostatic actuation principles. Conceptually, the electrostatic valve is the same as the pneumatic microvalve, but it contains an electrode embedded in the deflecting membrane and another electrode patterned on the bottom of the microfluidic channel. The membrane is shut by applying an electric field rather than using pneumatic pressure. The idea has been difficult to implement however. Quake *et al.* attempted to pattern an electrode on a sheet of thermoplastic (polyimide), and set the electrode on top of the PDMS membrane used for deflection [21]. They only achieved actuation after applying more than a kilovolt of potential, however. Maharbiz *et al.* fabricated electrostatic microvalves with a UV-curable form of PDMS and incorporated gold electrodes into the deflecting membrane [22, 23]. They were able to actuate their valves by applying potentials as low as 15 V, but the fabrication of the valves comprised many patterning, etching, and thermal annealing steps which significantly increased the complexity of fabrication. Juncker *et al*. developed an alternative procedure for constructing the valves by first depositing gold electrodes onto a thin PDMS membrane and then laminating the membrane onto glass microchannels [24]. The fabrication procedure was also relatively intensive, however, compared to the pneumatic precedent.

### 1.3 Objectives

In this work, I present an electrostatically actuated microvalve that is fabricated exclusively with soft-lithographic techniques. The valve is composed only of PDMS and conducting nanoparticles, and should be amenable to integration and also accommodate effective electrical controls. I report the development of an analytical model to guide the design of electrostatic microvalves, several methods that were investigated for embedding conducting nanoparticles in elastomeric membranes, and the subsequent fabrication of the microvalve. Initial tests were performed to characterize the electric potentials needed to actuate the microvalve, and I compare these results with the analytical model developed in this thesis. I also present a characterization of isolation pressures when the valves are actuated in air, and then preliminary results of actuation in oil and water.

## 1.4 Figures

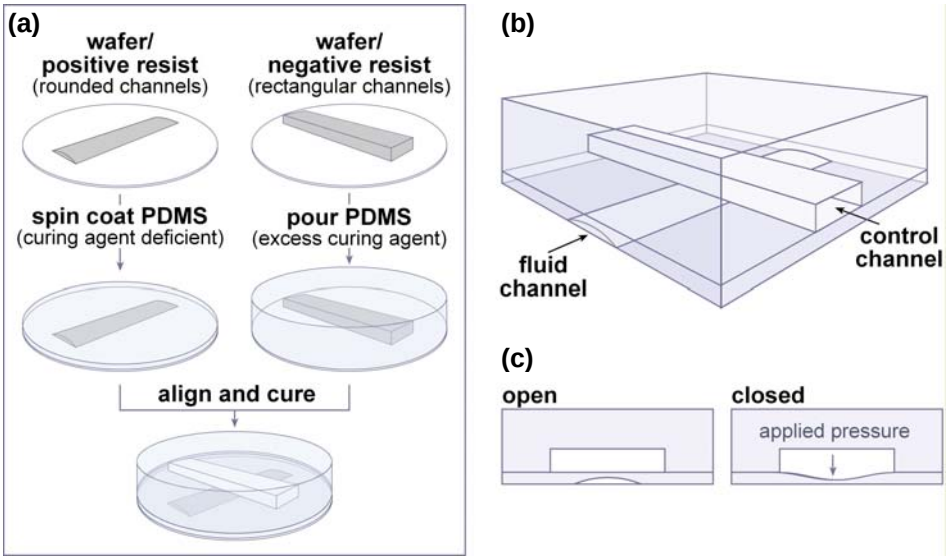


**Figure 1.1** Pneumatic microvalves made with soft-lithographic techniques [20]. Shown schematically are (a) the fabrication procedure for the valve, (b) valve cross-sections, and (c) the actuation of the valve with pneumatic pressure.

# Chapter 2: Development of Design Rules for Electrostatic Microvalves

## 2.1 Introduction

The operation of electrostatic microvalves involves several physical phenomena – most importantly the coupling between mechanical deformation and electric fields. The complex interplay of these phenomena necessitates a systematic model to describe the operation of the valve and guide the design process. While early efforts were being made towards a fabrication procedure for the valves, Dr. Amit Desai developed an analytical mathematical model to guide the subsequent optimization of the valve design with the objective of minimizing actuation potentials while maintaining fabrication simplicity and feasibility. The main conclusions from his analysis are presented in this chapter.

Two approaches are most commonly used in the modeling of electrostatic actuation of microscale structures: (i) numerical techniques and (ii) analytical or semi-analytical approaches. In the former approach, finite element analysis or numerical analysis of the governing differential equations are used to examine the deflection of compliant structures due to electrostatic forces. Using this approach, several studies have analyzed various phenomena during electrostatic actuation, including the dynamics of pull-in behavior [25, 26], the effect of large deformations and non-linear material properties [27], and Casimir forces [28]. However, the non-explicit representation of the design parameters and the complexity of these computational procedures limit the utility of these numerical models for the design of new electrostatic actuator configurations. In contrast, analytical and semi-analytical approaches describe the physical relationships between all the geometrical, material, and operational parameters explicitly. This

methodology has been used to model electrostatic actuation in various microscale applications, including actuation of micro-electromechanical systems in liquids [29] and electrostatic measurements of material properties [30]. It is also the methodology we decided would be most suitable for optimizing the microvalve geometry.

## 2.2 Results and Discussion

I first outline the main elements of Dr. Desai's derivation of the model, and afterward, I highlight the most important design parameters that affect actuation potential and the design space appropriate for our particular objectives.

### 2.2.1 Analytical Model

The microvalve is modeled as a parallel-plate capacitor where the electrodes are separated by a distance $g$ (Figure 2.1). One plate is movable, representing a deflecting membrane, and is attached to a spring with spring constant $k$. The parameter $y$ represents the displacement of the membrane and the extension of the spring. First, Dr. Desai derived expressions for the spring constant of the membrane based on plate theory [31]. Next, he calculated the actuation potential for a parallel-plate capacitor system using the spring constant expressions and energy-balance equations.

The derivation for the spring constant involves several expressions for the stiffness of a membrane. These are derived based on the following assumptions: (i) the membrane is homogenous, uniformly thick, and perfectly clamped at the outer edges, (ii) the deformation of the membrane is elastic, and (iii) membrane displacement due to transverse shear is negligible. The last assumption holds if the aspect ratio of the

membrane, i.e. the ratio of the diameter to the thickness, is greater than 5 [31]. For the microvalve discussed here, the aspect ratio will generally be greater than 10.

When the deflection of a membrane exceeds half its thickness, in-plane stresses are induced in the membrane. Membranes for microfluidic valves may deflect over distances significantly greater than their thickness. These in-plane stresses cause the membrane to be stiffer than that predicted by standard expressions for membrane stiffness. Hence, we introduce a correction factor, $K_{MS}$, to account for these effects of membrane stresses based on an approximation by Timoshenko and Woinowsky-Krieger [31]. The expression for static stiffness of a circular membrane that is fixed or clamped along the outer edges under a uniformly distributed load is given by

$$k = \frac{K_{MS}}{K_{AR}}\left( K^{1}_{shape}\frac{E_{bm}{t_m}^{3}}{D^{4}} + K^{2}_{shape}\frac{\sigma_0 t_m}{D^{2}}\right), \qquad (1)$$

where

$k$ static stiffness of the membrane per unit area

$E_{bm}$ biaxial modulus of the membrane and is given by $E_{bm} = \frac{E_m}{1-{\nu_m}^{2}}$

$E_m$ Young's modulus of the membrane material

$\nu_m$ Poisson's ratio of the membrane material

$t_m$ thickness of the membrane

$\sigma_0$ residual stress in the membrane

$D$ diameter of the membrane

$K^{1}_{shape}$ and $K^{2}_{shape}$ membrane shape factors

$K_{AR}$ factor to account for aspect ratio and is given by $K_{AR} = 1 + \frac{16}{1-\nu_m}\left(\frac{t_m}{D}\right)^{2}$ [31]

$K_{MS}$ factor to account for membrane stresses and is given by $K_{MS} = 1 + 0.488\left(\frac{g}{t_m}\right)^2$ [31].

In equation (1), the effect of stiffness of the conducting layer on the overall membrane stiffness is neglected, which is not necessarily true for the valves discussed here. A correction factor needs to be introduced into the expression for membrane stiffness for a significantly stiff conducting layer. The resulting expression for membrane stiffness is given by

$$k = K_{bilayer}\frac{K_{MS}}{K_{AR}}\left(K^1_{shape}\frac{E_{bm}{t_m}^3}{D^4} + K^2_{shape}\frac{\sigma_0\left(t_m + t_c\right)}{D^2}\right), \quad (2)$$

$$K_{bilayer} = 1 + \frac{E_c{t_c}^3\left(1-{\nu_m}^2\right)}{E_m{t_m}^3\left(1-{\nu_c}^2\right)} + \frac{3\left(1-{\nu_m}^2\right)\left(1+t_c/t_m\right)^2\left(1+E_m t_m/E_c t_c\right)}{\left(1+E_m t_m/E_c t_c\right)^2 - \left(\nu_m + \nu_c E_m t_m/E_c t_c\right)^2}$$

where

$K_{bilayer}$ factor to account for bilayer configuration [32]

$E_{bc}$ biaxial modulus of the conducting layer, given by $E_{bc} = \frac{E_c}{1-{\nu_c}^2}$

$E_c$ Young's modulus of the conducting material

$\nu_c$ Poisson's ratio of the conducting material

$t_c$ thickness of the conducting layer.

After deriving an expression for the spring constant, it can be used to find an expression for the potentials needed to collapse the valve. When considering the electrostatic component of the model, two main assumptions are made: (i) the fringing electric fields around the edges of the plates are assumed to be negligible, and (ii) the

electric field is assumed to be constant throughout the deformation of the membrane**.** Fringing electric fields do not significantly influence the capacitance between parallel plates when the electrode gap is small compared to the planar dimensions of the plate [33, 34], which is true for the valves reported here. The second assumption is valid only when the deflection of the membrane is insignificant compared to the electrode gap. In our system, deflections are nearly as large as the entire initial electrode separation, so this discrepancy needs to be addressed. Calculating the actual deflection profile of the membrane would entail numerical solution of non-linear partial differential equations or multi-physics simulations using finite element analysis (FEA). Alternatively, the actuation potential value can be multiplied by a constant, $K_{nonlinear}$, to capture the influence of the non-uniform electric field. This $K_{nonlinear}$ can be estimated numerically or experimentally. Osterberg *et al*. computed $K_{nonlinear}$ as 0.7545 using FEA simulations [30], while Rollier *et al*. assumed $K_{nonlinear}$ as 1 and observed a maximum difference of 6% between analytical predictions and experimental observations for actuation potentials [29]. In this paper, we assume $K_{nonlinear}$ to be equal to 1, realizing that this assumption induces an error of 10% or less in the analytical predictions of actuation potentials.

In parallel plate actuators, the system becomes unstable when the electrostatic forces and restoring mechanical forces are no longer in equilibrium [29]. Beyond a certain deflection, the membrane collapses suddenly or snaps in. This phenomenon of snap-in is known as the pull-in instability. The critical deflection is given by

$$y_{snapin} = \frac{1}{3}\left( h_c \frac{\varepsilon_{fluid}}{\varepsilon_m} + g \right), \qquad (3)$$

where $\varepsilon_{fluid}$ and $\varepsilon_m$ are the relative permittivity of the fluid and membrane, respectively, and $h_c$ is the thickness of the dielectric insulating layer between the upper electrode and the channel (Figure 2.1). Depending on the relative magnitudes of the critical deflection and the initial gap between the plates, the operation of the electrostatic valve is either in the stable deflection regime (i.e. critical deflection is never reached) or governed by the aforementioned pull-in instability (i.e. the critical deflection is exceeded). If $y_{snapin} > g$, the electrostatic valve is in the stable deflection regime and the actuation potential required to close the valve is given by

$$V_{close} = \sqrt{\frac{2kg\left(h_c \frac{\varepsilon_{fluid}}{\varepsilon_m}\right)^2}{\varepsilon_0 \varepsilon_{flluid}}}, \qquad (4)$$

where $\varepsilon_0$ is the permittivity of free space and the membrane stiffness $k$ is given by either equation (1) or (2). If $y_{snapin} \leq g$, the actuation of the valve is governed by pull-in instability, and the potential required to close the valve is given by

$$V_{close} = \sqrt{\frac{8k\left(g + \left(h_c \frac{\varepsilon_{fluid}}{\varepsilon_m}\right)\right)^3}{27\varepsilon_0 \varepsilon_{fluid}}}. \qquad (5)$$

### 2.2.2 Design Space

To identify the design space for the electrostatic microvalves, equations (1), (2), (4), and (5) were first used to ascertain the scaling relations between actuation potential and model parameters, with higher order corresponding to greater influence. The data in Table 2.1 show that the actuation potential is most sensitive to changes in membrane

diameter, $D$, membrane thickness, $t_m$, and electrode gap, $g$, as expected. Less intuitive is the relation between the actuation potential and the dielectric properties of the fluid. Based on data in Table 2.1, an increase in the dielectric constant of the fluid will not necessarily decrease the actuation potential. This counter-intuitive observation is due to the non-negligible thickness of the dielectric insulating layer, $h_c$, and finite value for the dielectric constant of this layer.

After identifying the crucial parameters, the parameters were used to define the design space that would accommodate low actuation potentials accessible with compact power sources, such as a DC power supply or battery pack. Figure 2.2 shows the design parameter space with respect to aspect ratio ($D/t_m$) and relative gap ($g/t_m$), for a valve actuated in air with actuation potentials lower than 50 V. Values for non-variable parameters used in this analysis are listed in Table 2.2. Figure 2.2 predicts that actuation potentials as low as 15 V can be obtained while maintaining dimensions for the membrane diameter, membrane thickness, and channel height that are feasible from a fabrication point of view. Based on the model and also several known design constraints, the explicit design space is tabulated in the last column of Table 2.1.

## 2.3 Conclusions

Using a semi-analytical approach, we developed a model to predict actuation potentials for electrostatic microvalves. The model identified valve diameter, membrane thickness, and electrode gap to be the most influential parameters affecting actuation potentials, and we were able to approximate the design space with these parameters that would lead to low actuation potentials of 50 V or less. Other important phenomena are

also involved in the operation of electrostatic microvalves, such as squeeze-film damping and adhesion-driven valve collapse, and will be the subject of future modeling work.

## 2.4 Figures and Tables

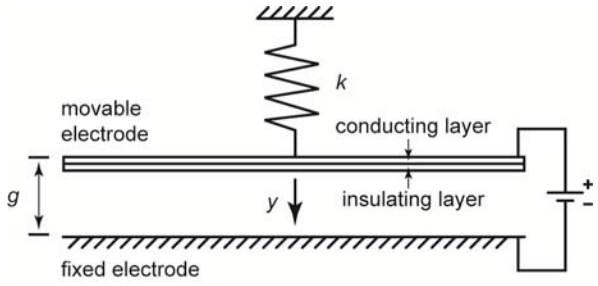


**Figure 2.1** Schematic representation of the parallel plate actuator used to mathematically model the electrostatic microvalve.

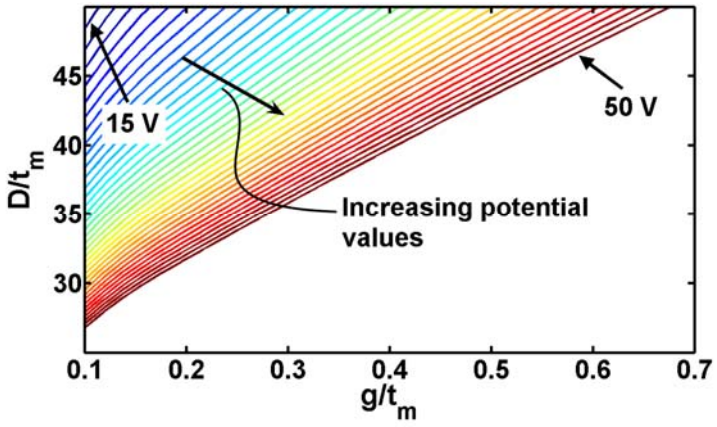


**Figure 2.2** Design parameter space for electrostatic valves with actuation potentials below 50 V. Each contour line corresponds to a different actuation potential, ranging from 15 to 50 V in 1 V steps.

**Table 2.1** The most influential parameters affecting microvalve actuation potentials and the approximate design space leading to microvalves with actuation potentials below 50 V.

| **Parameter** | **Order of dependency** | | **Design range** |
|---|---|---|---|
| | *Stable region* | *Snap-in* | |
| Diameter, $D$ | -2 | -2 | 300-1000 μm |
| Membrane thickness, $t_m$ | 2.5 | 3 | 10-50 μm |
| Electrode gap, $g$ | 0.5 | 1.5 | 1-15μm |
| Dielectric constant of fluid, $\varepsilon_{fluid}$ | 0.5 | 1 | -- |

**Table 2.2** Values of valve parameters used when defining the design space for the electrostatic valves.

| **Parameter** | **Value** |
|---|---|
| $E_m$ | 0.7 [35] |
| $\nu_m$ | 0.5 [35] |
| $\varepsilon_m$ | 2.75 [36] |
| $\sigma_0$ | 0.1 MPa [37, 38] |
| $K^1_{shape}$ | 85.33 [39] |
| $K^2_{shape}$ | 16 [40, 41] |
| $E_c$ | 1.6 [42] |
| $\nu_c$ | ~ 0.5 |
| $t_c$ | 0.1 μm |
| $h_c$ | 10 μm |

# Chapter 3: Design and Optimization of Conducting Elastomeric Membranes

## 3.1 Introduction

The central component of our microvalve design is a flexible, conducting, elastomeric membrane. We chose to use PDMS as the elastomeric material because it is easily molded from liquid precursors via a platinum catalyzed vinyl addition and also extensively used in the literature. However, conferring conductivity to PDMS is not always straightforward. Metals are notoriously difficult to pattern on PDMS because most thermal and sputtering depositions heat the polymer and cause it to expand. When the PDMS cools, the metallic films buckle [43]. Even if metallic films are patterned successfully onto PDMS without buckling, the films cannot sustain large strains without breaking. Conducting polymers could be used instead of PDMS or in tandem with PDMS, but they are usually more difficult to process, and many exhibit plastic rather than elastomeric deformation [44]. Consequently, we decided to address the problem by embedding conducting nanoparticles into PDMS membranes, retaining the simple processing of PDMS but also enabling large deflections without loss of conductivity. In all, we explored three different approaches for patterning conducting nanoparticles in PDMS: (i) directly mixing the nanoparticles into the elastomer precursors prior to processing, (ii) airbrushing nanoparticles onto a pre-existing membrane, and (iii) forming a film of nanoparticles by filtration and subsequently transferring the film to a PDMS membrane via microtransfer printing.

## 3.2 Results and Discussion

### 3.2.1 Nanoparticle/Polymer Composites

We initially attempted to embed nanoparticles in uncured PDMS and then process the slurry into a thin membrane suitable for deflection. Some precedents for this approach were found in the literature, though mainly for the creation of elastomeric electrical sensors rather than actuators [45]. Liu *et al*. embedded multi-walled carbon nanotubes (MWNT) into PDMS precursors and then used the slurry to fill the gaps of a mold of photoresist [46]. Residual slurry was removed with a razor blade, and after curing, the photoresist was removed with a suitable solvent. By using this "doctor-blading" technique, the researchers were able to pattern micron-sized structures of the conducting elastomer. The researchers found that MWNT possessed a favorable percolation threshold (concentration or particle loading at which electrical conductivity is established) compared with spherical conducting nanoparticles such as carbon black. This lower percolation threshold is due to the large aspect ratio of the MWNT, which improves the probability of adjacent particles making contact. Consequently, for most of the initial studies reported here, MWNT were used as the conducting material in our membranes.

We adopted Liu's approach and patterned photoresist around large rectangular regions on a silicon wafer, filled the recess with a MWNT/PDMS slurry (usually 10 wt% MWNT), and then slid a razor blade across the rectangular region, using the photoresist to effectively define the height of the MWNT/PDMS membrane. Carbon nanotubes were >95 wt% purity, <1.5 wt% ash, and had 20-40 nm outer diameter and 10-30 μm length (Cheap Tubes Inc.). While the resulting membranes were conductive, we encountered

several difficulties. First, streaking caused non-uniformities in membranes. This streaking may have been due to the large lengths of the nanoparticles compared to the thickness of the membrane (the MWNT we used were as long as 30 μm, which was about as thick as or thicker than the photoresist mold). The streaking also could have been caused by the roughness of the razor blade, aggregates of the MWNT, or the speed at which the blade was drawn across the mold. Second, the thickness of the membranes was difficult to control, perhaps due to uneven pressure applied by the blade. Lastly, the concentration of nanoparticles in the slurry increased the stiffness of the membrane, and estimates from our model predicted that we would need to compensate by fabricating membranes significantly thinner than what was experimentally possible.

It should also be noted that we tried to make membranes by pressing the MWNT/PDMS slurry onto a substrate rather than doctor-blading, but in this process, the MWNT tended to clump together and prevent thin, smooth films from forming. From these initial observations, we decided that embedding MWNT directly into PDMS precursors was not advantageous and decided to direct efforts towards patterning MWNT thin films onto PDMS membranes that were already formed.

### 3.2.2 Airbrushed Nanoparticle Films

We next attempted to airbrush a solution of MWNT directly onto a PDMS membrane. Conductive MWNT films have been airbrushed onto various surfaces such as glass and plastics for photovoltaic applications [47]. The films can be made thin enough to be transparent, in contrast to the doctor-blading approach where the membranes were

opaque. Having transparent electrodes would be advantageous for several reasons, including visualizing flow inside the valves or taking optical measurements.

MWNT were suspended in an aqueous solution with the aid of a surfactant, sodium dodecyl sulfate (SDS), and separately, PDMS was spin-coated onto a silicon wafer and fully cured. Afterward, the aqueous solution of MWNT and SDS was airbrushed as evenly as possible onto the surface. After certain threshold coverage was achieved, the films conducted, and if properly masked, we imagine that the films could be patterned.

We also encountered difficulties with this approach, however. When observed under the microscope, the films had noticeable surface heterogeneities. Literature suggests that this is due to the rate of evaporation from the aerosols emitted from the airbrush [48]. If the solvent evaporates too quickly before the solution reaches the substrate, then the MWNT aggregate before being deposited. Alternatively, if the solution does not adequately evaporate before reaching the substrate, then liquid droplets form on the surface of the substrate, leading to uneven deposition of MWNT.

Another problem emerged when trying to encapsulate the MWNT film with a second layer of PDMS. Surfactant that was deposited along with the MWNT prevented additional layers of PDMS from sealing to underlying layers, and the membranes easily delaminated.

### 3.2.3 Microtransfer Printing of Nanoparticle Films

In our experience, both doctor-blading and air-brushing failed to yield conducting MWNT/PDMS membranes that were sufficiently smooth and uniform for application in

the electrostatic microvalve. Filtration of a MWNT suspension, however, was previously shown to yield highly uniform, conductive, and transparent films [48]. It was also shown that these films could be transferred to various substrates either by applying pressure and heat or by dissolving the filter with an appropriate solvent.

To adopt the procedure for our purposes, MWNT were suspended in an aqueous solution, again with the addition of SDS. Typically, solutions were made in a ratio of 1 mg MWNT and 10 mg SDS per 1 mL water. The solution was sonicated approximately 30 min. to break up MWNT aggregates and subsequently centrifuged to isolate any bundles that could not be disintegrated. The solution was then filtered through a membrane, typically with a pore size of 0.2 μm. A uniform black film was formed on the filter resulting in a soapy, clear and colorless filtrate. After the solution was completely filtered, the film was washed with alcohol (isopropyl alcohol, methanol, or ethanol) until the filtrate was free of any bubbles. After drying, the MWNT film could be transferred directly to a pre-formed PDMS membrane.

Several filter materials were investigated for suitability for transferring MWNT films. Teflon® filters released MWNT films relatively easily; however, Teflon® filters with small pore sizes were delicate and were manufactured with a polyethylene support mesh on the underside. This mesh produced a texture in the MWNT film, and in extremely thin films, the mesh caused discontinuities. Nylon, cellulose, polycarbonate, and polyester filter membranes were also investigated. However, none of these materials transferred MWNT films reliably, unless the film was thick and non-transparent. Usually, the top layers of the MWNT film would transfer, leaving a textured residual film behind. Filter membranes that consistently yielded the best results were composed of

alumina (Whatman Anopore inorganic membranes). MWNT films could be completely transferred, even if very thin, leaving behind hardly any visible residue. It should be noted, however, that the inorganic membranes were brittle and had to be handled more carefully than the polymeric membrane filters.

We performed several characterization studies of conducting PDMS membranes fabricated in the above manner. Firstly, we quantified the dependence of resistivity on MWNT loading with no strain applied to the membrane (Figure 3.1a). Resistivity decreased and converged to a value of ~1 Ohm-cm as MWNT loading increased and reached a value of ~0.5 mg/cm$^2$. The gradual conferral of conductivity with particle loading is a result of the large aspect ratio of the MWNTs. There was no clearly defined percolation threshold, but we are confident that percolation occurs at or below 0.3 g/cm$^2$, allowing us to fabricate functional electrodes that are semi-transparent.

Next, we applied a slow, periodic strain (60%, 2 hrs/cycle) to the membrane and observed the change in resistance (Figure 3.1b). The resistance increased as strain increased, but remained conductive until rupture. We did not observe any mechanical or electrical hysteresis during the stretch tests. These data demonstrate the advantage of using polymer/nanoparticles composites compared to metallic films on polymer, because significantly higher strains are accessible without compromising electrode integrity.

We also applied rapid strains to the membrane and observed that after an initial increase, the resistance undergoes a transient reduction proportional to the induced strain and then levels off (Figure 3.1c). We assume that this behavior is due to the reorientation of the MWNT in the polymer after a rapid deformation. At this point, it is not clear

whether this will either benefit or detract from the quality of operation of the valve, but it is an interesting observation.

After finding a suitable technique of conferring conductivity to elastomeric membranes, the next challenge was to develop a way to pattern the conducting areas. Microcontact printing proved to be an easy yet highly effective solution [49]. After MWNT were filtered to form a thin film, a patterned PDMS stamp (20 PDMS monomer: 1 PDMS cross-linker weight ratio, hereafter referred to as 20:1 PDMS) was brought into conformal contact with the film, slight pressure was applied by hand, and then the stamp was removed along with the selected areas of the film. When the stamp was pressed onto a PDMS membrane, the MWNT were transferred onto the new substrate. For the transfer to happen reliably, the PDMS membrane was also made of 20:1 PDMS, although it was not cured to the same degree, ensuring that the receiving surface was tackier than the stamp. Membranes or slabs of PDMS with different weight ratios of cross-linker were also capable of receiving the MWNT film from the PDMS stamp, but again, the substrates were under-cured so that they were tackier than the stamp. If the receiving PDMS membrane was too tacky, the stamp and membrane tended to adhere too strongly to be separated. We were able to create patterns as small as 50 μm wide, although we believe smaller features are possible. With this particular technique, we can make the complex circuitry needed for arrays of independently operated valves.

### 3.3 Conclusions

Overall, filtration and microtransfer printing produced a conducting membrane that proved most amenable for adaptation into an electrostatic microvalve. We can tune

the loading of nanoparticles to control the conductivity of the film and make electrodes that are semi-transparent. The film retains conductivity over large deflections, and there is little observable mechanical or electrical hysteresis due to the PDMS deformation. Transparent films should be beneficial for visualizing fluid flow through microvalves or detecting analytes.

## 3.4 Figures

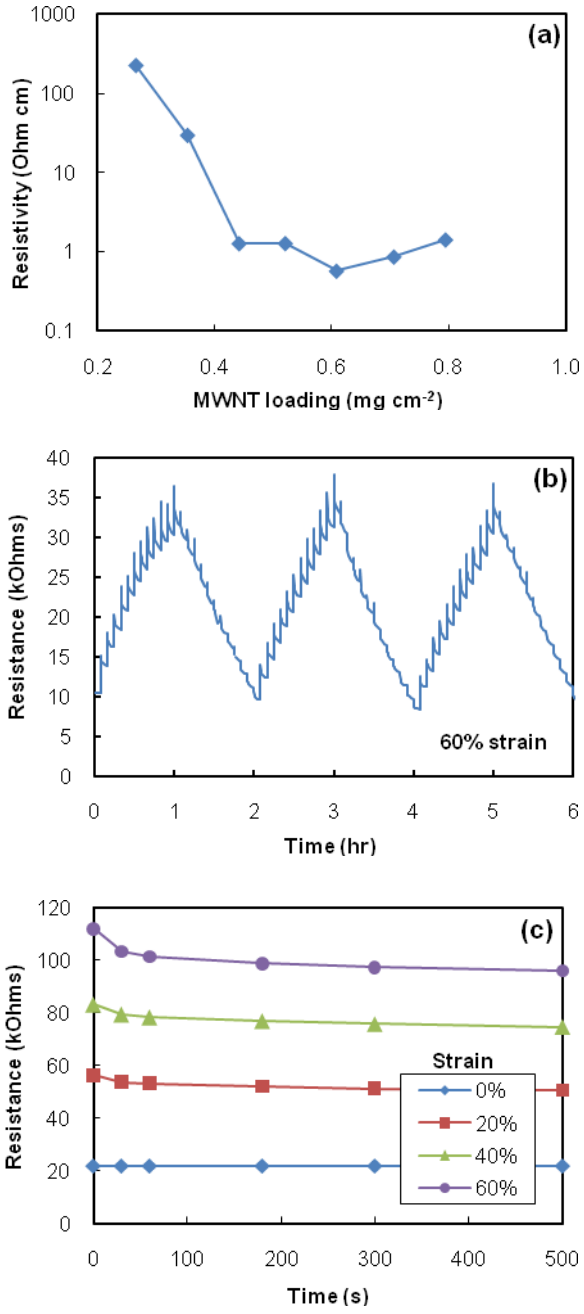


**Figure 3.1** Characterization of PDMS membranes with MWNT electrodes. (a) Measured resistivity as a function of MWNT loading in an unstrained membrane. (b) Electrical response of a membrane undergoing a 60% strain at a rate of 0.5 cycle/second. (c) Electrical response of rapidly strained membranes.

# Chapter 4: Design and Optimization of Arrays of Electrostatic Microvalves

## 4.1 Introduction

After devising an appropriate means of fabricating conducting membranes with patterned electrodes, the next challenge was to integrate the membranes into complete microvalve assemblies. However, the fabrication entailed more than a simple lamination of the membrane on top of microfluidic channels. We developed a fabrication procedure that allowed us to create microfluidic channels (and in the future, other microfluidic components) in parallel with the microvalves by implementing simple replica molding techniques along with the microtransfer printing.

Following the fabrication, our main objective was to minimize the actuation potential of the microvalve, assuring that microvalve could be implemented in portable microchemical systems. Towards this end, we used Dr. Desai's mathematical model to identify the design space that would be appropriate and then varied several of the design parameters to optimize the actuation potentials. Before this could be accomplished however, we had to address several unseen issues, including the sagging of membranes.

In this chapter, I first give a detailed procedure for the fabrication of the microvalves followed by a discussion of support structures that were implemented to prevent membranes from collapsing prematurely. I then discuss the process whereby actuation potentials were minimized to values as low as 5 V. The chapter concludes with cursory studies of valve isolation pressures and actuation in liquid media.

## 4.2 Experimental Methods

### 4.2.1 Microvalve Fabrication

Figure 4.1 shows a schematic diagram of the fabrication process flow. Molds for microfluidic channels and the supporting layers of the devices were made from patterned photoresist on silicon. Masks were designed with Adobe® Illustrator® and printed onto film with a high resolution printer (5080 dpi) from University of Illinois printing services. Typically, negative photoresist was processed according to manufacturer specifications (SU8-5 and SU8-50 for fluid layers and support layers, respectively; Microchem Corp.) To systematically fabricate microvalves with different channel heights, we needed to adjust the height of the features on the microfluidic channel mold, but the manufacturer did not provide spin-curves with the range of heights we required. Our own spin-curve calibration data for SU8-5 are presented in Figure 4.2. Features on the molds for the microfluidic channels were typically 1-10 μm tall, and features for the support layers were 50 μm tall. After development, the mold was treated with a vapor of (tridecafluoro-1,1,2,2-tetrahydro octyl)-1-trichlorosilane (United Chemical Technologies, Inc.) by placing the wafer in a vacuum desiccator for four hours with several drops of the silane. The vacuum line passed through a column of solid sodium hydroxide pellets to neutralize gaseous hydrochloric acid resulting from the reaction.

To create the upper portion of the electrostatic microvalve, liquid PDMS precursors (GE RTV 615, purchased through Hisco-Schaumburg) were dispensed in a ratio of 20:1 base/curing-agent by weight (20:1 PDMS), and after mixing, the PDMS was degassed in a vacuum desiccator for several minutes until no bubbles were visible. A thin layer of PDMS was spin-coated onto the mold for microfluidic channels at 10,000

rpm. This layer formed the insulating layer of the membrane between the channel and electrode to be deposited later. The thickness of this layer depended on the height of the mold features and the length of spin-coating. In our preliminary work, we used spin-rates that were slower than ideal, typically around 7000 rpm, which resulted in thick insulating layers of ~10μm (and consequently higher actuation potentials). A calibration for mold features 2.1, 4.0, and 6.4 μm high is presented in Figure 4.3. We found that the thinnest insulating layer that could be fabricated for all three channel heights was 2 μm, and this height was used for our latest results for actuation potential optimization. The initial PDMS layer was cured in an oven at 70$^{o}$C for 30 min before applying the MWNT electrode.

To form the electrode, a MWNT film was patterned onto the insulating PDMS layer via microcontact printing. A stock solution of MWNT was made in a ratio of 1 mg MWNT / 10 mg SDS / 1 mL 18 MΩ water. MWNT were >95 wt% purity, <1.5 wt% ash, and had 20-40 nm outer diameter and 10-30 μm length (Cheap Tubes Inc.). Both MWNT and SDS (Fisher Scientific) were used without further purification. The solution was placed in an ultrasonic bath for 30 min. and then centrifuged at 4000 rpm for 15 min. to remove unwanted aggregates. Between 1-3 mL of the MWNT solution was vacuum filtered through an alumina membrane filter with 0.2 μm pore size (Anopore inorganic membranes, Whatman). In the latest iteration of this fabrication process, the MWNT solution was first diluted with 50 mL 18 MΩ water prior to filtration, leading to more uniform films. Following filtration, the resulting MWNT film was washed with methanol, ethanol, or isopropanol until the filtrate was clear, colorless, and without

bubbles. The film was allowed to dry for several minutes under ambient conditions, and then transferred with a PDMS stamp.

The stamp was made by pouring 20:1 PDMS over a silicon/photoresist mold and curing at 70$^{o}$C for at least one hour, but usually overnight. To transfer the MWNT film, the stamp was brought into conformal contact with the film and slight pressure was applied by hand. When removed, the stamp picked up the selected areas of the MWNT film, and this MWNT pattern was aligned and set onto the previously formed PDMS layer. Again, pressure was applied by hand, and the stamp was peeled off the PDMS layer, leaving the MWNT film behind.

A homogeneous slurry of MWNT and 5:1 PDMS (~10 wt% MWNT) was made by repeatedly drawing the mixture over a surface with a razor blade. The slurry was then applied onto peripheral regions of the exposed MWNT film to serve as electrical contacts. The high concentration of curing-agent in the PDMS served to minimize curing time, which was ~5 min. at 70 $^{o}$C.

Next, a layer of 20:1 PDMS was spin-coated onto the MWNT film typically at 2400 rpm for 30 s with a 10 s ramp. This increased the membrane thickness by ~30 μm, but the spin-rate and spin time could be varied to yield membranes of different thicknesses. This layer served both as an encapsulating layer for the MWNT electrode and as an adhesion layer for the support layer. To properly adhere to the support layer, the adhesion layer was heated at 70 $^{o}$C for 20-30 min. or until just slightly tacky. The support layer was formed by pouring liquid 5:1 PDMS over a mold and curing at 70 $^{o}$C for at least 15 min. (Longer cure times up to an hour also gave good results.) After, both layers were aligned and brought into conformal contact. If certain regions were

misaligned, the layers could be de-sealed and then realigned without negative effects. Surplus vinyl groups in the adhesion layer reacted with excess silicon hydrides in the support layer during the final cure of at least 60 min. at 70 $^{o}$C. During this step, extra liquid PDMS was poured around the support layer and over the electrical contacts to fill in any gaps. The device was removed from the mold by cutting around the appropriate areas with a scalpel.

When quantifying the actuation potential required to close the valves, we used a lower electrode made of a thin film of indium tin oxide (ITO) on glass. For studies of fluid flow in the valves, however, the lower electrode was fabricated out of PDMS and sealed permanently to the upper electrode.

The substrate used for creating the lower PDMS electrode was a polished silicon wafer treated with (tridecafluoro-1,1,2,2-tetrahydro octyl)-1-trichlorosilane in the same manner as the molds. A slurry of 20:1 PDMS and MWNT (~10 wt% MWNT) was mixed together with a razor blade and small amounts were dispensed on the silicon to serve as electrical contacts. A ~0.5 cm thick layer of 20:1 PDMS was poured onto the substrate and heated in an oven at 70 $^{o}$C for 20-30 min until the PDMS was slightly tacky. The slab of PDMS was cut out with a scalpel, and a MWNT film was microtransfer printed onto the underside (the side originally oriented against the silicon). Care was taken to insure that the MWNT film overlapped with the electrical contacts in the PDMS slab. The slab was then pressed down into the silicon substrate so that the MWNT film was directly against the silicon. When pressure was applied, the MWNT film appeared to turn darker, indicating that the PDMS slab was sufficiently sealed against the silicon surface. The slab was fully cured by heating at 70 $^{o}$C for at least one

hour without any applied pressure. When ready for use, the slab was simply peeled off the substrate.

To seal the upper electrode and lower PDMS electrode together permanently, both elements were treated with plasma and then aligned together. First, access holes were punched to the microfluidic channels with a sharpened needle. Both the upper and lower electrode were placed onto frosted glass slides and set in a plasma cleaner (Harrick Plasma, Extended model). Glass slides provided a rigid support for the PDMS components to rest on while the roughness of the surface prevented the glass from sealing to the PDMS. The chamber was evacuated to 500 mTorr of atmospheric gases, and exposed to plasma under the "high" setting for 90 s. After exposure, the two halves were aligned, gently brought into contact, and then heated at least one hour at 70 $^{o}$C.

### 4.2.2 Microvalve Characterization

To actuate the microvalves, the electrodes were attached to a high voltage DC power source with the lower electrode positively polarized and the membrane negatively polarized. For lower electrodes comprising ITO on glass, the electrode was directly attached to the power source with an alligator clip and lead wire. PDMS electrodes were attached by stabbing a wire into the PDMS/MWNT contacts and then attaching an alligator clip to the wire. The potential was gradually increased until valves collapsed. Valve collapse was observed visually under a microscope.

## 4.3 Results and Discussion

### 4.3.1 General Observations of Microvalve Actuation

Figure 4.4 shows both schematics and micrographs of valves before and after being actuated with an electrostatic force. In most of our experiments, we tested an array of microvalves with diameters ranging between 200-1000 μm in diameter with 100 μm increments. As the potential between the electrodes was gradually increased, the membrane of a valve deflected until it reached a critical deflection. After surpassing a threshold potential, the valve immediately snapped shut within milliseconds. For the quantification of actuation potentials, most of the channels had rectangular cross-sections, and there was a noticeable region around the peripheries of the valve where the membrane did not seal completely. In separate experiments with channels that had rounded cross-sections, however, we observed that the valves sealed hermetically.

In the initial study of actuation potentials, an ITO/glass lower electrode was used. The adhesion energy between smooth oxide surfaces and PDMS is strong, and after actuation, most of the valves remained shut even after the electric potential was released. In some cases, however, the elastic energy stored in the membrane was enough to peel the membrane off the lower electrode and return it to the rest state.

### 4.3.2 Implementation of Membrane Support Structures

Initially, the valve membranes had the tendency to sag after being removed from their molds, and this often led to premature valve collapse before actuation potentials were applied. Additionally, the sag in the membranes probably contributed to the issue of valves staying shut. Above a certain aspect ratio, elastomeric membranes will collapse naturally [50], but we observed that normally stable aspect ratios still led to collapse.

This result is probably related to the mismatch between thermal expansion coefficients in the PDMS and MWNT layers of the membrane. We attempted to cure all the membrane layers at room temperature, but our initial attempt did not completely eliminate the problem.

As an alternate means of preventing premature membrane collapse, support structures were molded into the support layer for the valves and sealed to the top side of the membranes during fabrication. Several different geometries were tested for the support structures, including posts, spirals, and triangular beams. Usually, larger valves were still prone to premature collapse ( $\geq$ 700 μm diameter), but the structures did ameliorate the problem partially.

Actuation potentials that correspond to several different support structures are shown in Figure 4.5. (Channel height was ~2 μm; the insulating layer of PDMS in the membrane was ~10 μm; the encapsulating layer was ~40 μm; and the total thickness of the membrane was ~50 μm). Currently, there are not adequate data to clearly distinguish the effects of different geometries of the support structures. However, the actuation data show a general trend that was typical for most of the experiments reported here. As the diameter of the microvalve increased, the actuation potential tended to decrease and converge asymptotically to a minimal actuation potential.

We performed a more systematic study of one particular support structure geometry – a single post. We varied the width of the post in comparison with the diameter of the microvalve, ranging from 50-100% of the diameter. All of the posts were 50 μm tall. Figure 4.6 shows that as the post size increased, so did the actuation potential needed to close the valve. With posts widths that were 50% of the diameter of the valve,

valves actuated with as little as 20V. However, larger posts were most effectual in preventing premature collapse of the membranes.

### 4.3.3 Effect of Elastic Modulus of Support Structures on Actuation Potentials

To implement large support structures but also achieve low actuation potentials, we attempted to decrease the elastic modulus of the support structures above the membranes. We created a support layer with a support post 100% the diameter of the valve – essentially a solid slab of PDMS. We used different ratios of monomer to cross-linker in the support layers and found, predictably, that less cross-linked layers led to lower actuation potentials (Figure 4.7). Valves with a support slab fabricated out of 5:1 PDMS actuated in the proximity of 300 V. By increasing the amount of monomer relative to cross-linker, we achieved actuation with as little as 40 V for a valve with 40:1 PDMS in the support layer. However, with ratios higher than 20:1, the support layer became increasingly tacky. After valves actuated, adjacent channels would close as well. In addition, if the support layer did not contain an excess of cross-linker, the support layer could not be effectively sealed to the membrane.

After investigating the geometry and elasticity of the support structures, we decided to use a post 20% the diameter of the valve and fabricated out of 5:1 PDMS for further work since it reduced the likelihood of premature membrane collapse, led to the lowest actuation potentials for all the geometries tested, and could still be sealed easily to the underlying membrane.

### 4.3.4 Optimized Actuation Potentials and Comparison with Model

To simultaneously optimize the actuation potential of the microvalve and investigate the accuracy of our model, we systematically varied several parameters in the valve fabrication. We made arrays of microvalves with channel heights of 2.1, 4.0, and 6.4 μm and tested two membrane thicknesses of ~20 and ~40 μm. The insulating layer of PDMS between the upper electrode and the microfluidic channel was ~2 μm thick for all valves.

Results of our investigation are shown in Figure 4.8. As expected, smaller gaps between electrodes, thinner membranes, and larger diameters all led to lower actuation potentials. Our model is accurate within a factor of two, but tends to underestimate the potential needed to actuate the valves. This could be due to several reasons, including the effect of support structures on the membrane stiffness, greater residual stresses in the membrane than predicted, or variations in the thickness of the insulating layer of the membranes. Especially for larger valves, the first layer of spun-on PDMS tended to bulge up near the center of mold structures, effectively increasing the distance between electrodes.

More importantly, the optimization of the valve design yielded actuation potentials as low as 5 V. With potentials this low, it may eventually become possible to directly integrate the microvalves with electrical integrated circuits (ICs) rather than having to operate the valve and its controls with different potentials.

### 4.3.5 Isolation Pressures

In the results presented in Figure 4.8, only three of the valves tested were able to reopen. The two valves with 200 μm diameters and 6.4 μm channel heights reopened as well as the valve with 200 μm diameter, 4.0 μm channel height, and 40 μm membrane thickness. All these valves were actuated with a potential of at least 150 V. We hypothesized that switching to a PDMS/MWNT lower electrode would decrease the surface adhesion between the membrane and the lower electrode and allow valves to reopen. Using a PDMS/MWNT lower electrode also enabled us to seal the two electrodes together permanently and flow fluids through the channels. We anticipated that the fluids would help lubricate the surface or at least be able to push the valves open if an external pressure was applied.

The new surface did not greatly decrease the propensity of the valves to remain shut, but we were able to open the valves when applying pressure to the air in the channels. Figure 4.9 shows the pressure needed to reopen a 500 μm wide valve (2 μm tall channel, 10 μm insulating layer of PDMS, ~50 μm thick membrane) in relation to the applied potential. The valve reopened with very little applied pressure, which suggests that the adhesion energy between the membrane and lower electrode is far from insurmountable. However, the valves are currently not optimized for applications that require high isolation pressures.

### 4.3.6 Actuation with Fluids

We also actuated the valves with fluorinated oil (3M™ Fluorinert™ FC-40) and 18 MΩ water in the channels. Valves reopened more easily when they contained FC-40

as opposed to air (e.g. valves with diameters larger than 200 μm were able to open), but isolation pressures were much lower. (We were unable to accurately measure the pressures with our current equipment). The lowest actuation potential for a valve that reopened with the MWNT/PDMS lower electrode and containing FC-40 was 150 V.

With water, we were unable to completely close the valves. This may have been due to dilute ions in the water that assembled at the electrode surfaces when a potential was applied and screened the electric field. Others have circumvented this problem by using high frequency AC potentials [22, 51], and we are currently investigating the efficacy of using these AC potentials with our system.

### 4.4 Conclusions

In summary, we developed a simple procedure to fabricate arrays of microvalves using only replica molding and microtransfer printing. To prevent membrane sagging, we incorporated support structures into the valve design and investigated the effects of geometry and elastic modulus of these structures on actuation potential. After optimizing the valve design parameters, we were able to achieve actuation potentials as low as 5 V, and our results agree well with the predictions from the analytical model. Valves reopen when fluids in the channels are pressurized beyond a certain threshold. In the case of water, valves do not actuate completely because charged solutes assemble at the electrodes and screen DC electric fields. This electrode screening may be prevented by rapidly switching the polarity of the electric field, but several obstacles need to be addressed first and will be the focus of future work.

## 4.5 Figures

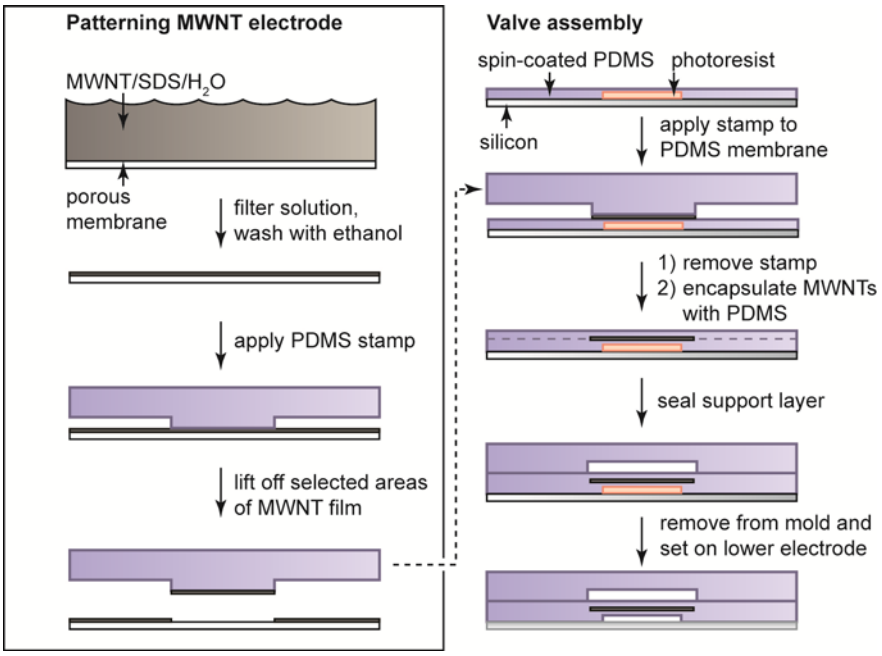


**Figure 4.1** Schematic diagram of the reported soft-lithographic approach of fabricating electrostatic microvalves.

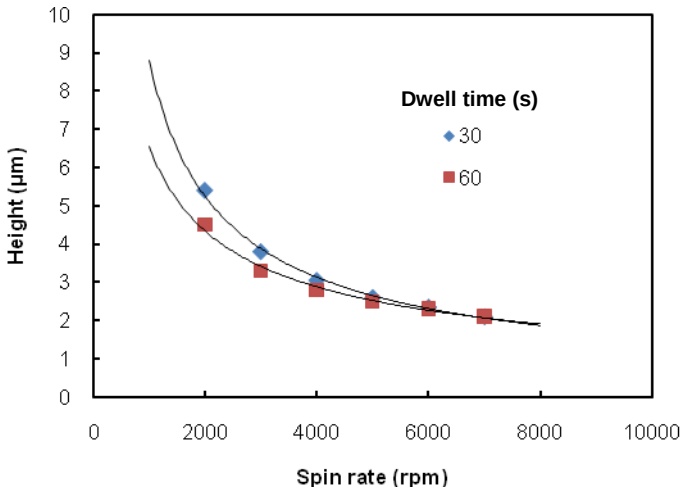


**Figure 4.2** Spin curves for SU8-5 negative photoresist.

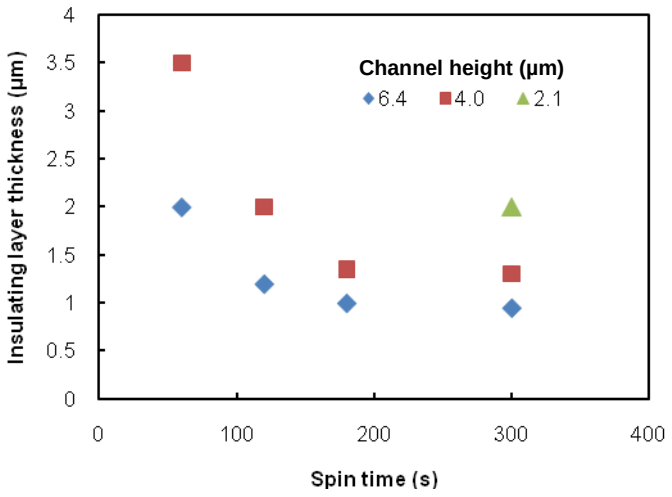


**Figure 4.3** Calibration of PDMS film thickness above SU8 structures after spin-coating at 10,000 rpm for different times.

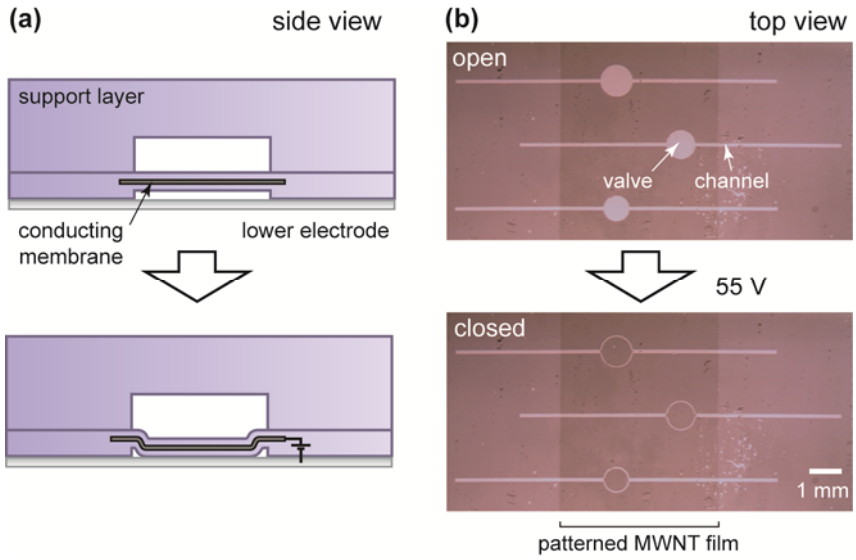


**Figure 4.4** Microvalve actuation with electrostatic forces. (a) Schematic illustration of membrane collapse due to an applied potential. (b) Micrographs of microvalves in the open state initially and then in the closed state after applying a 55 V potential.

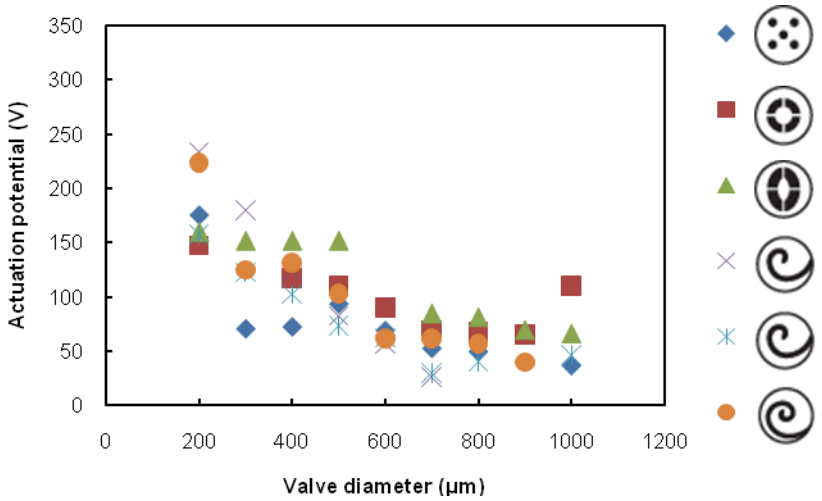


**Figure 4.5** Actuation potentials corresponding to valves with different support structures. Channel height was ~2 µm; the insulating layer of PDMS in the membrane was ~10 µm; the encapsulating layer was ~40 µm; and the total thickness of the membrane was ~50 µm.

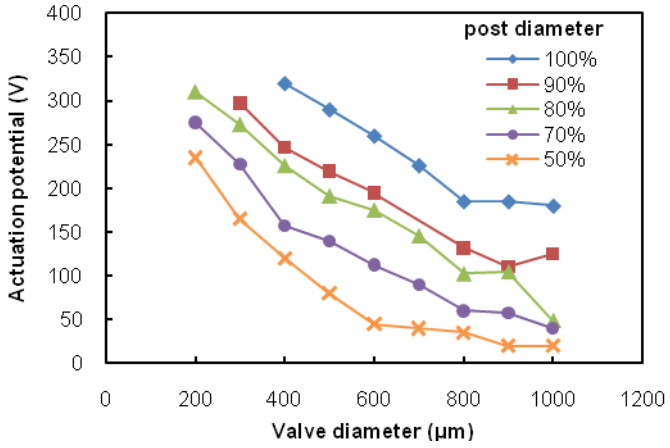


**Figure 4.6** Actuation potentials corresponding to valves with a single post as a support structure. The diameter of the post is recorded as a certain percentage of the width of the valve.

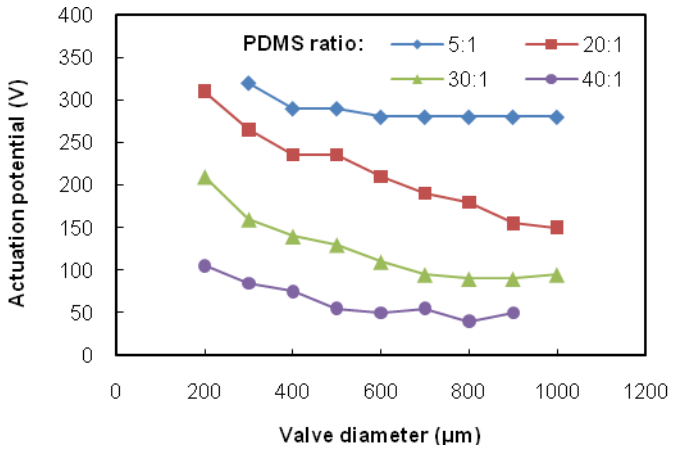


**Figure 4.7** Actuation potentials corresponding to valves with support layers made of different ratios of PDMS monomer to crosslinker. The support structure was a solid slab of PDMS that completely covered the top side of the membrane.

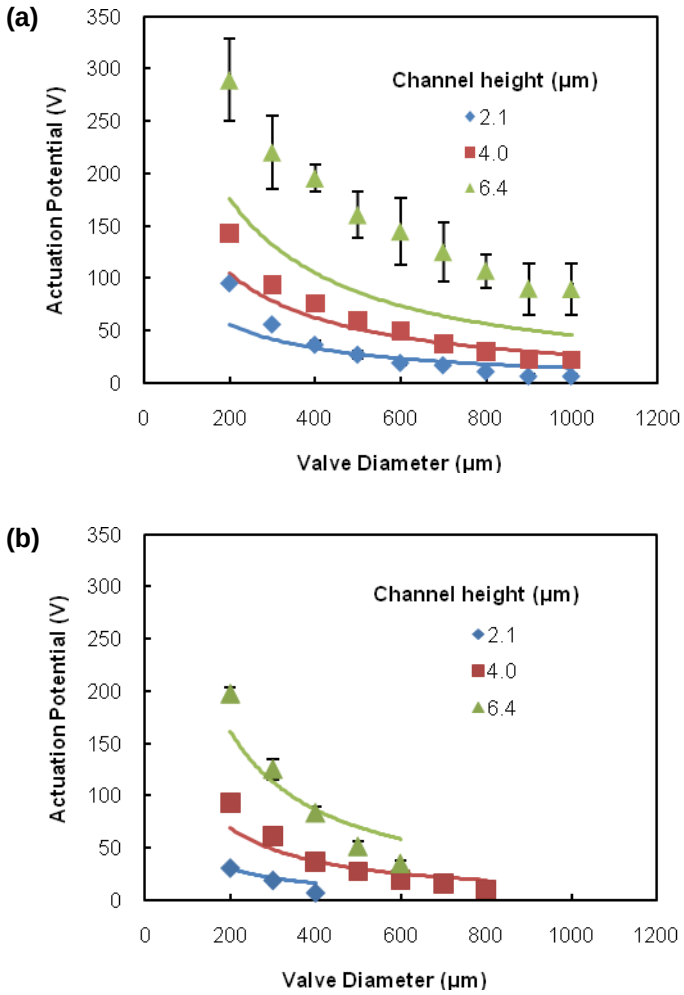


**Figure 4.8** Systematic variation of electrode separation, membrane thickness, and valve diameter and the effect on actuation potential. (a) Valves with ~20 µm thick membranes. (b) Valves with ~40 µm thick membranes. Each set of valves had an insulating layer of PDMS ~2 µm thick between the top of the channel and the upper electrode. Experimental results are shown as points and model predictions are shown as lines. Scale bars represent one standard deviation.

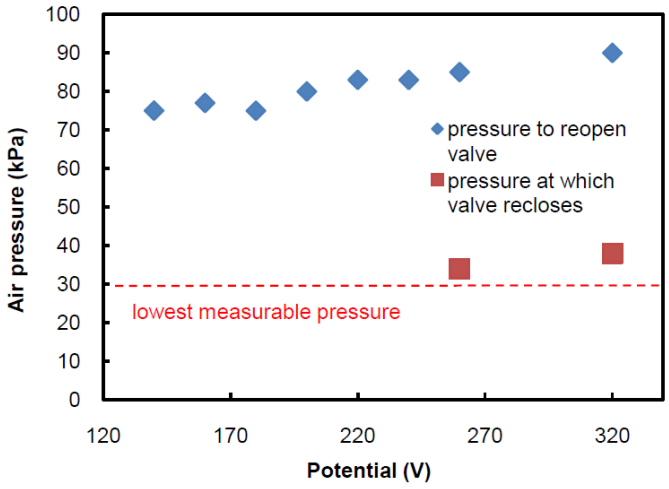


**Figure 4.9** Isolation pressures for a 500 µm diameter valve. The actuation potential of the valve under atmospheric pressure was 75 V. The valve contained a 2 µm tall channel, 10 µm insulating layer of PDMS, and ~50 µm thick membrane. A potential was applied to close the valve, then pressure was gradually increased until the valve reopened. After, the pressure was decreased until the valve re-shut.

# Chapter 5: Concluding Remarks

## 5.1 Summary

In conclusion, we developed an electrostatically actuated microvalve fabricated solely with the soft lithographic techniques of replica molding and microtransfer printing. The fabrication can be performed under ambient conditions, and no specialized deposition or etching tools are required. The valves are monolithically integrated with the rest of the device, and valves as small as 200 μm in diameter were created. For larger valves that were prone to premature collapse, we investigated a number of different support structures and eventually implemented a single post that held the membrane up prior to actuation but still allowed for low actuation potentials.

Our analytical model accurately predicted actuation potentials within a factor of two and also identified the most important parameters influencing valve actuation. By optimizing these parameters, we were able to construct valves that actuated with as little as 5 V. Though the valves tended to remain shut after actuation, especially on ITO/glass lower electrodes, they could be easily reopened by pressurizing the air or fluid in the channel. We were able to actuate the valves in air and oil, but dilute ions in aqueous media screened the electrical potential between the electrodes and prevented actuation with DC fields.

## 5.2 Future Work

Several aspects need to be addressed before the microvalve reaches its full utility and can be effectively integrated into complete microchemical systems. First of all, the

inability of the microvalve to return to the open state without external pressure being applied is a noticeable disadvantage. One way to address this problem would be to pattern raised structures on the valve seat that would either reduce the contact area between the elastomeric membrane and the lower electrode or add additional strain to the membrane, thus conferring greater restoring force. There is also the possibility of performing a surface modification to the membrane, the valve seat, or both that would decrease the adhesion between them. Several fluorinated compounds, such as Cytop®, have been used to treat PDMS channels and may help improve membrane release.

The problem of membrane stiction is only exasperated by the sag in the membranes, particularly in membranes larger than 500 μm in diameter. There is still potential that this problem could be solved by curing the membrane completely at room temperature, giving no occasion for the PDMS to expand under elevated temperatures. However, more scrutiny should be lent to the thickness of the various layers composing the membrane in addition to the stresses induced during spin-coating.

The residual stresses in the membrane may also decrease the model's accuracy in predicting actuation potentials. If this is the case, then a procedure needs to be developed to directly measure these stresses so that more accurate assumptions can be incorporated into the model.

Finally, the inability of the valve to operate in aqueous environments with DC potentials needs to be addressed. Electric fields with rapidly oscillating polarity need to be implemented to prevent the screening of electrodes, but several criteria need to be met by the circuit. The capacitance of the microvalve must be relatively small so that charges can quickly saturate the surfaces of the electrodes and create a substantial electrostatic

force. At the same time, the resistance of the circuit must be low so that charges can move quickly between electrodes. Currently, the resistance of the MWNT electrodes is too high, so different conducting nanoparticles with higher conductivity need to be used. We are currently investigating gold nanoparticles as an alternative, but there are several challenges associated with patterning gold nanoparticles via microtransfer printing. Carbon nanotubes are hydrophobic and adhere well to PDMS stamps, but gold nanoparticles are naturally hydrophilic, and cannot be picked up reliably with PDMS stamps. Surface treatment of the PDMS stamp or the nanoparticles may be necessary to print with the same reliability as MWNT. In addition, there are only a few publications that report the fabrication of gold nanoribbons or nanobelts that are similar to MWNT in terms of aspect ratios [52, 53]. Spherical nanoparticles require significantly higher particle loadings to achieve the percolation threshold, so we are currently investigating gold nanoplates and gold nanorods. The effort is necessary, however, since the most relevant media for biological applications tend to be aqueous media with high ionic content.

Following the completion of the valve, we anticipate that the societal benefit of the proposed technology will be especially valuable if the microvalves can be integrated into point-of-care diagnostic systems. A future manifestation of the technology might include a hand-held device capable of processing patient blood or DNA in automated fashion, eliminating the need for a highly trained technician or specialized facilities. Since the valves consume little power, they could also be integrated into long term wireless chemical detection systems to augment public security.

# Chapter 6: References


[1] N. T. Nguyen and Z. G. Wu, "Micromixers - a review", Journal of Micromechanics and Microengineering, 2005, 15, R1-R16.

[2] H. Yan, B. Y. Zhang and H. K. Wu, "Chemical cytometry on microfluidic chips", Electrophoresis, 2008, 29, 1775-1786.

[3] D. Di Carlo, "Inertial microfluidics", Lab on a Chip, 2009, 9, 3038-3046.

[4] S. Tia and A. E. Herr, "On-chip technologies for multidimensional separations", Lab on a Chip, 2009, 9, 2524-2536.

[5] D. J. Laser and J. G. Santiago, "A review of micropumps", Journal of Micromechanics and Microengineering, 2004, 14, R35-R64.

[6] P. Watts and S. J. Haswell, "The application of micro reactors for organic synthesis", Chemical Society Reviews, 2005, 34, 235-246.

[7] H. R. Sahoo, J. G. Kralj and K. F. Jensen, "Multistep continuous-flow microchemical synthesis involving multiple reactions and separations", Angewandte Chemie-International Edition, 2007, 46, 5704-5708.

[8] V. Taly, B. T. Kelly and A. D. Griffiths, "Droplets as microreactors for high-throughput biology", Chembiochem, 2007, 8, 263-272.

[9] P. Watts and C. Wiles, "Recent advances in synthetic micro reaction technology", Chemical Communications, 2007, 443-467.

[10] Y. H. Zhang and P. Ozdemir, "Microfluidic DNA amplification-A review", Analytica Chimica Acta, 2009, 638, 115-125.

[11] R. D. Johnson, V. G. Gaualas, S. Daunert and L. G. Bachas, "Microfluidic ion-sensing devices", Analytica Chimica Acta, 2008, 613, 20-30.

[12] J. Mairhofer, K. Roppert and P. Ertl, "Microfluidic Systems for Pathogen Sensing: A Review", Sensors, 2009, 9, 4804-4823.

[13] B. M. Paegel, R. G. Blazej and R. A. Mathies, "Microfluidic devices for DNA sequencing: sample preparation and electrophoretic analysis", Current Opinion in Biotechnology, 2003, 14, 42-50.

[14] M. Diehn, R. W. Cho, N. A. Lobo, T. Kalisky, M. J. Dorie, A. N. Kulp, D. L. Qian, J. S. Lam, L. E. Ailles, M. Z. Wong, B. Joshua, M. J. Kaplan, I. Wapnir, F. M. Dirbas, G. Somlo, C. Garberoglio, B. Paz, J. Shen, S. K. Lau, S. R. Quake, J. M. Brown, I. L. Weissman and M. F. Clarke, "Association of reactive oxygen species levels and radioresistance in cancer stem cells", Nature, 2009, 458, 780-U123.

[15] C. C. Lee, G. D. Sui, A. Elizarov, C. Y. J. Shu, Y. S. Shin, A. N. Dooley, J. Huang, A. Daridon, P. Wyatt, D. Stout, H. C. Kolb, O. N. Witte, N. Satyamurthy, J. R. Heath, M. E. Phelps, S. R. Quake and H. R. Tseng, "Multistep synthesis of a

radiolabeled imaging probe using integrated microfluidics", Science, 2005, 310, 1793-1796.

[16] C. L. Hansen, E. Skordalakes, J. M. Berger and S. R. Quake, "A robust and scalable microfluidic metering method that allows protein crystal growth by free interface diffusion", Proceedings of the National Academy of Sciences of the United States of America, 2002, 99, 16531-16536.

[17] M. J. Anderson, C. L. Hansen and S. R. Quake, "The use of microfluidic devices towards protein crystallography", Biophysical Journal, 2005, 88, 55A-55A.

[18] M. J. Anderson, C. L. Hansen and S. R. Quake, "Phase knowledge enables rational screens for protein crystallization", Proceedings of the National Academy of Sciences of the United States of America, 2006, 103, 16746-16751.

[19] K. W. Oh and C. H. Ahn, "A review of microvalves", Journal of Micromechanics and Microengineering, 2006, 16, R13-R39.

[20] M. A. Unger, H. P. Chou, T. Thorsen, A. Scherer and S. R. Quake, "Monolithic microfabricated valves and pumps by multilayer soft lithography", Science, 2000, 288, 113-116.

[21] B. S. Driggs, M. M. Enzelberger and S. R. Quake, "Electrostatic Valves for Microfluidic Devices", U. S. Patent 10/045,132, Filed October 23, 2001

[22] T. Bansal, M. P. Chang and M. M. Maharbiz, "A class of low voltage, elastomer-metal 'wet' actuators for use in highdensity microfluidics", Lab on a Chip, 2007, 7, 164-166.

[23] M. P. Chang and M. M. Maharbiz, "Electrostatically-driven elastomer components for user-reconfigurable high density microfluidics", Lab on a Chip, 2009, 9, 1274-1281.

[24] D. Juncker, M. Nannini and V. Logiudice, "Electrical Microvalve and Method of Manufacturing Thereof", I. Patent PCT/CA2007/001997, Filed May 11, 2007.

[25] G. Flores, G. Mercado, J. A. Pelesko and N. Smyth, "Analysis of the Dynamics and Touchdown in a Model of Electrostatic MEMS", SIAM Journal on Applied Mathematics, 2007, 67, 434-446.

[26] Y. Guo, Z. Pan and M. J. Ward, "Touchdown and Pull-In Voltage Behavior of a MEMS Device with Varying Dielectric Properties", SIAM Journal on Applied Mathematics, 2005, 66, 361.

[27] N. C. Goulbourne, M. I. Frecker and E. Mockensturm, "Electro-elastic modeling of a dielectric elastomer diaphragm for a prosthetic blood pump", Smart Structures and Materials 2004: Electroactive Polymer Actuators and Devices (EAPAD), San Diego, CA, USA.

[28] C. Wang, W. Guo and Q. Feng, "Deflection and stability of membrane structures under electrostatic and Casimir forces in microelectromechanical systems", Acta Mechanica, 2005, 180, 49-60.

[29] A. S. Rollier, B. Legrand, D. Collard and L. Buchaillot, "The stability and pull-in voltage of electrostatic parallel-plate actuators in liquid solutions", Journal of Micromechanics and Microengineering, 2006, 16, 794-801.

[30] P. M. Osterberg and S. D. Senturia, "M-TEST: A Test Chip for MEMS Material Property Measurement Using Electrostatically Actuated Test Structures", Journal of Microelectromechanical Systems, 1997, 6, 107-118.

[31] S. Timoshenko and S. Woinowsky-Krieger, "Theory of Plates and Shells", New York: McGraw-Hill Book Company, 1959.

[32] W. C. Young, "Roark's formulas for stress and strain ", New York: McGraw-Hill, 2002.

[33] M. Hosseini, G. Zhu and Y.-A. Peter, "A new formulation of fringing capacitance and its application to the control of parallel-plate electrostatic micro actuators", Analog Integrated Circuits and Signal Processing, 2007, 53, 119-128.

[34] B. Palmer, "Capacitance of a parallel-plate capacitor by the Schwartz- Christoffel transformation", Transactions on AIEE, 1937, 56, 363 -366.

[35] D. Armani, D. Armani, C. Liu and N. Aluru, "Re-configurable fluid circuits by PDMS elastomer micromachining", Twelfth IEEE International Conference on Micro Electro Mechanical Systems, MEMS '99.

[36] "Sylgard 184 silicone elastomer data sheet", http://www1.dowcorning.com/DataFiles/090007c8801d3f9e.pdf, 09/21/2009.

[37] M. Maghribi, J. Hamilton, D. Polla, K. Rose, T. Wilson and P. Krulevitch, "Stretchable micro-electrode array for retinal prosthesis", 2nd Annual International IEEE-EMB Special Topic Conference on Microtechnologies in Medicine & Biology.

[38] A. Thangawng, R. Ruoff, M. Swartz and M. Glucksberg, "An ultra-thin PDMS membrane as a bio/micro–nano interface: fabrication and characterization", Biomedical Microdevices, 2007, 9, 587-595.

[39] M. D. Giovanni, "Flat and Corrugated Diaphgram Design Handbook", New York: Marcel Dekker Inc., 1982.

[40] M. K. Small and W. D. Nix, "Analysis of the accuracy of the bulge test in determining the mechanical properties of thin films", Journal of Material Research, 1992, 7, 1553 - 1563.

[41] J. J. Vlassak and W. D. Nix, "A new bulge test technique for the determination of Young's modulus and Poisson's ratio of thin films", Journal of Materials Research, 1992, 7, 3242 - 3249.

[42] J. Paul, S. Sindhu, M. H. Nurmawati and S. Valiyaveettil, "Mechanics of prestressed polydimethylsiloxane-carbon nanotube composite", Applied Physics Letters, 2006, 89, 184101-3.

[43] N. Bowden, S. Brittain, A. G. Evans, J. W. Hutchinson and G. M. Whitesides, "Spontaneous formation of ordered structures in thin films of metals supported on an elastomeric polymer", Nature, 1998, 393, 146-149.

[44] P. Chandrasekhar, "Conducting polymers, fundamentals and applications: a practical approach", Boston: Kluwer Academic, 1999.

[45] C. H. Hu, C. H. Liu, L. Z. Chen, Y. C. Peng and S. S. Fan, "Resistance-pressure sensitivity and a mechanism study of multiwall carbon nanotube networks/poly(dimethylsiloxane) composites", Applied Physics Letters, 2008, 93, 3.

[46] C. Liu, "Recent developments in polymer MEMS", Advanced Materials, 2007, 19, 3783-3790.

[47] M. Kaempgen, G. S. Duesberg and S. Roth, "Transparent carbon nanotube coatings", Applied Surface Science, 2005, 252, 425-429.

[48] Z. C. Wu, Z. H. Chen, X. Du, J. M. Logan, J. Sippel, M. Nikolou, K. Kamaras, J. R. Reynolds, D. B. Tanner, A. F. Hebard and A. G. Rinzler, "Transparent, conductive carbon nanotube films", Science, 2004, 305, 1273-1276.

[49] Y. Zhou, L. Hu and G. Gruner, "A method of printing carbon nanotube thin films", Applied Physics Letters, 2006, 88, 123109.

[50] K. J. Hsia, Y. Huang, E. Menard, J. U. Park, W. Zhou, J. Rogers and J. M. Fulton, "Collapse of stamps for soft lithography due to interfacial adhesion", Applied Physics Letters, 2005, 86, 154106-3.

[51] T. L. Sounart, T. A. Michalske and K. R. Zavadil, "Frequency-dependent electrostatic actuation in microfluidic MEMS", Journal of Microelectromechanical Systems, 2005, 14, 125-133.

[52] M. S. Bakshi, F. Possmayer and N. O. Petersen, "Aqueous-phase room-temperature synthesis of gold nanoribbons: Soft template effect of a gemini surfactant", Journal of Physical Chemistry C, 2008, 112, 8259-8265.

[53] N. Zhao, Y. Wei, N. J. Sun, Q. J. Chen, J. W. Bai, L. P. Zhou, Y. Qin, M. X. Li and L. M. Qi, "Controlled synthesis of gold nanobelts and nanocombs in aqueous mixed surfactant solutions", Langmuir, 2008, 24, 991-998.